DE GRUYTER Open Physics 2025; 23: 20250136

Research Article

Adel M. El Sayed* and Faisal Katib Alanazi*

Tuning the structure and electro-optical properties of α-Cr_2O_3 films by heat treatment/La doping for optoelectronic applications

https://doi.org/10.1515/phys-2025-0136
received October 23, 2024; accepted March 04, 2025

Abstract: Controlling the physicochemical features of chromium sesquioxide α-Cr_2O_3 (chromia) films is essential to widening their utilization. This work investigates the influence of heat treatment (HT) and La doping on the physical characteristics of chromia films spin-deposited on glass. X-ray diffraction/Fourier transform infrared spectroscopy and field-emission transmission electron microscopy techniques reveal that the crystallinity, size, and modes of vibration in chromia (eskolaite phase) can be tuned by HT and La doping. Energy-dispersive X-ray analysis confirms the presence of La in the hexagonal chromia films. All films display high transmittance (T%) and improved absorption indices in the UV and near-infrared regions. The films' reflection and refractive indices are in the range of 6–15% and 1.77–1.97, respectively. The impact of HT and La content on the optical band gap, lattice dielectric constant, and electron-effective mass is reported. The current–voltage characteristic curves reveal the Ohmic resistance, and the films' sheet resistance demonstrates sensitivity to HT and La content. The findings of this study illustrate the possible development of optoelectronic devices and chromia-based IR sensors.

Keywords: α-Cr_2O_3, band gap engineering, optical constants, La doping, I–V characteristics

1 Introduction

Various cutting-edge technologies, such as green energy, energy storage, networks, and superconductivity, have some form of metal oxide coatings or thin films [1]. Metal oxides are fascinating multifunctional materials that could be introduced in various technological applications. The filled *s*-shells acquire good chemical and thermal stability, and their partially filled *d*-shells provide interesting electronic properties [2]. Among the metal oxides, chromium sesquioxide (α-Cr_2O_3 or chromia) is an attractive multifunctional material due to its low cost (wide availability), low humidity dependency, good chemical and color stability, high thermal stability and corrosion resistance, and adjustable band structure [3]. Chromia is an antiferromagnetic insulator with a Neel temperature of 307 K (34°C) [4]. These properties make chromia suitable for several applications, such as a hard coating or protection layer for tools and machines for high-temperature applications [5]. According to Tian *et al.* [6], adding 0.1% chromia to ZnO-based varistor ceramics improves I–V nonlinearity and reduces the leakage current. Owing to its interesting photoelectric properties, Li *et al.* [7] suggested the use of microfibers decorated with chromia, grown by magnetron sputtering, as a saturable absorber for ultrafast fiber laser technology. Alotabi *et al.* [8] used the photo-deposited chromia layer on different material particles to prevent the reverse reaction in photocatalytic water splitting.

A fundamental step in the application of chromia coatings is controlling the synthesized material by adjusting the processing technique [9]. In other words, the preparation technique and preparative parameters determine the physicochemical and biological features of chromia nanoparticles (NPs) and thin films, and introducing foreign atoms (dopants) can enhance and broaden these features. Heating $Cr(NO_3)_3$ at above 350°C in KOH solution resulted in green nano-crystalline Cr_2O_3 pigments for reflection purposes in the wavelength region 750–2,500 nm [10]. Tsegay *et al.* [11] utilized drop-casting and spin-coating to obtain

---

*** Corresponding author: Adel M. El Sayed,** Department of Physics, Faculty of Science, Fayoum University, El-Fayoum, 63514, Egypt, e-mail: ams06@fayoum.edu.eg

*** Corresponding author: Faisal Katib Alanazi,** Department of Physics, College of Science, Northern Border University, Arar, 73222, Saudi Arabia, e-mail: Fisal.Alanazi@nbu.edu.sa

ORCID: Adel M. El Sayed 0000-0002-6544-3844; Faisal Katib Alanazi 0000-0002-9478-2394

quasi-spherical, nanorod, and meso-spherical-shaped chromia that can act as a spectrally selective solar absorber. The pulsed-laser deposited (PLD) Ni-doped chromia films showed improved photoresponse for solar cells and photoelectrodes [12]. According to Erickson *et al.* [13], B doping and adjusting the Cr_2O_3/V_2O_3 film thickness, *via* PLD, can be used to increase the Neel temperature of Cr_2O_3 for voltage control due to its antiferromagnetic properties. The nano-sized Fe-doped chromia exhibited weak ferromagnetism and therefore can be used in logic and spintronic data storage devices [14]. In addition, Bhardwaj *et al.* [15,16] prepared chromia NPs by the co-precipitation method and found that doping with 10% Co and Mn can reduce the E_g value from 2.96 to 2.82 eV, or 2.51 eV, which made the doping materials useful for optoelectronic applications. Moreover, the PLD films made from these materials demonstrated p-type conductivity and room-temperature (RT) ferromagnetism, making them suitable for spintronic device applications. By covering chromia NPs made by the microemulsion method with Ni or Co NPs, Yıldırım [17] improved their specific capacitance and ability to store energy. The X-ray diffraction (XRD) peak intensities of Cr_2O_3 in the composites were greatly reduced compared with those of the uncovered Cr_2O_3 NPs. Furthermore, Gyawali *et al.* [3] prepared Ag/chromia NPs by liquid impregnation and annealing with enhanced antibacterial efficiency. Additionally, the Pd/chromia electrode prepared by reactive dc magnetron co-sputtering was found to be a viable candidate for utilization in supercapacitors as future energy storage devices [18].

According to Zekaik *et al.* [19], the E_g of 0.0–12 at% Cu-doped chromia in the dip-coated films reduced from ~2.9 to 2.5 eV and the resistance from 87 to 12.8 Ω. Ishtiaq *et al.* [20] found that the hardness of the chromia films deposited on soda lime glass substrates improved with Cu doping to 2.0%, and the antibacterial activity of the films increased with increasing Cu/Cr ratio. Bio-synthesized chromia NPs, 15–24 nm in size, showed E_g values in the range of 3.02–3.29 eV [21]. Furthermore, Ba inclusion was found to improve the rate of H_2 production of chromia from $NaBH_4$ methanolysis from 5,984 to 31,176 mL/g min at 15% Ba content [22].

The rare earth (RE) ions can form strong bonds with the metal oxide's functional groups due to the presence of 4*f* empty orbitals [23], and therefore RE dopants can alter the physical characteristics of chromia. A few reports on the effect of RE on the chromia films' features are recounted in the literature. Ikram *et al.* [23] studied the impact of Sr doping on the bactericidal potential and catalytic activity of nano-sized chromia for wastewater treatment. Jia *et al.* [5] used Y-doping and the ion-plating technique to fabricate chromia films with improved friction and wear resistance performance, as well as reasonable stability at high temperatures. The trivalent doping could induce vacancy complexes (vacant Cr sites proximal to oxygen vacancies), and these structural defects may encourage the researchers to develop spintronic devices based on Cr_2O_3 doped with La^{3+} [24]. In addition, the La electronic 4*f*–4*f* transitions result in strong emission peaks with wavelengths in the visible and infrared regions. This enhances the photoluminescence features of the host material for optoelectronic applications [25].

The current work aims to investigate the influence of HT and La doping on the structure and electrical and optical properties of chromia thin films, which have not been reported yet. Most of the physical and chemical synthetic techniques require specialized devices with high costs and high temperatures. However, the sol–gel preparation combined with the spin-coating technique is more affordable and cost-efficient [26]. The solutions were sol–gel-prepared and then spin-coated on glass substrates. The influence of HT/La doping on the structural and morphological features of the films was studied by XRD/Fourier transform infrared (FTIR) spectroscopy and field-emission scanning electron microscopy (FESEM) and energy-dispersive X-ray spectroscopy (EDAX/EDS). The results of optical and electrical properties revealed the possible development of these films for photoelectrooptical devices.

2 Experimental section

2.1 Film preparation

Chromium acetate ($Cr_2C_8H_{16}O_{10}$, ~376 g mol^{-1}, >97%; LOBA Chemie, India), 2-methoxyethanol ($C_3H_8O_2$, ~76 g/mol; Merck), and monoethanolamine (C_2H_7NO, ~61 g/mol; Merck) were used as the precursor, solvent, and stabilizer, respectively, for chromia thin film preparation. $LaCl_3.7H_2O$ (371.4 g/mol, >97%; WINLAB, India) was used for La doping. About 0.94 g of Cr source was dissolved in 10 mL of solvent (0.25 M) using a magnetic stirrer. Some drops of stabilizing agent were added during stirring for 1.0 h at 45°C until a clear and homogeneous solution was formed. To prepare 2.5 and 5.0 at% La-doped chromia films, the same procedure was repeated by adding the required mass of the La source. The solutions were kept at RT for 1 day. The glass substrates were washed with neat ethanol and neat water, 5 min for each, using an ultrasonic bath and then air dried. The prepared solutions were coated at 2,100 rpm for 25 s. The deposited (six) layers were pre-heated at 220°C on a hotplate for 5 min to yield films with

200–230 nm thickness. Finally, the samples were heat-treated at 400, 500, and 600°C for 2 h in a furnace. The La-doped films were also annealed at 600°C. The furnace was left to cool naturally to RT. In the following sections, the names (codes) of the samples will be Cr/400, Cr/500, Cr/600, 2.5% La-Cr/600, and 5.0% La-Cr/600.

2.2 Devices

An X'Pert Pro (PANalytical) XRD system was used to examine the phase structure, purity, and size of the spin-deposited chromia films. The surface morphology and elemental (chemical) composition were investigated using a ZEISS SUPRA 55-VP field-emission scanning electron microscope attached to an EDS unit. The chromia functional groups and vibration modes were studied by gathering the FTIR spectra using a VERTEX 70 Bruker spectrophotometer in the range of 400–4,000 cm^{-1}. The optical reflectance/transmittance (T%) in the 200–1,500 nm wavelength region was obtained using a UV-3600 Shimadzu spectrophotometer, in normal incidence mode. The reflectance spectrum was collected using an integrating sphere attachment, and a barium compound was used as reference for 100% reflectance. A Keithley-2400 unit was used for obtaining the current (I)–voltage (V) curves using the two-point probe method.

3 Results and discussion

3.1 Structural analysis (XRD, FTIR, and FE-SEM)

The structural properties of the coated chromia films that were annealed at 400–600°C and doped with La were investigated using the X-ray diffractometer in the 2θ range of 20–75° and applying a Cu K_α radiation source (wavelength: λ ~0.1541 nm). The obtained diffraction patterns are shown in Figure 1. The peak intensity grew significantly with the heat treatment (HT), indicating the improvement in crystallinity with HT at 400–600°C. The most significant peaks were observed at 2θ = 24.66, 33.57, 36.21, and 54.83°. However, doping with La reduced the peak intensity again, indicating deterioration of crystallinity; however, the Cr_2O_3 phase remained unaffected with doping. Similar patterns were obtained for undoped and Cu-doped chromia films prepared by spray pyrolysis on pre-heated (400°C) soda lime glass substrates [20]. In addition, increasing the ratio of the Y element shifted the chromia film toward the amorphous state [16]. According to Salari Mehr *et al.* [27,28], the crystallinity of the atomic layer-deposited (ALD) chromia films greatly improved and the eskolaite phase formed with the increase of the substrate temperature from 200 to 275°C but deteriorated upon the addition of Ti. According to Joshi *et al.* [29], doping with La content ≥ 4 at% La leads to the formation of a TiO_2 rutile structure as an additional phase alongside the anatase phase. In addition, loading of 0.1–0.3 at% La_2O_3 to ZnO–Bi_2O_3 microparticles through the flash-sintering route did not change the crystal structure (phase) of the varistor, and 0.2 at% La_2O_3 was enough to achieve a uniform structure with the highest density and best electrical efficiency [30]. These results indicate the possibility of controlling the chromia film crystallinity. The decrease in crystallinity correlated with an increase in defects and disorder within the materials. This will improve the film conductivity and optical characteristics, which will be covered in the following sections.

The analysis of the obtained data (the positions and relative intensities of the peaks) revealed that the formed material is a hexagonal chromia (α-Cr_2O_3, eskolaite phase) with a rhombohedral primitive cell (JCPDS nos 01-072-4555 and 01-084-0313 [26]). The Miller indices were inserted on all peaks. No trace related to La or its oxides was detected in the patterns. This outcome confirmed the purity of the product and aligned with the findings reported for La-

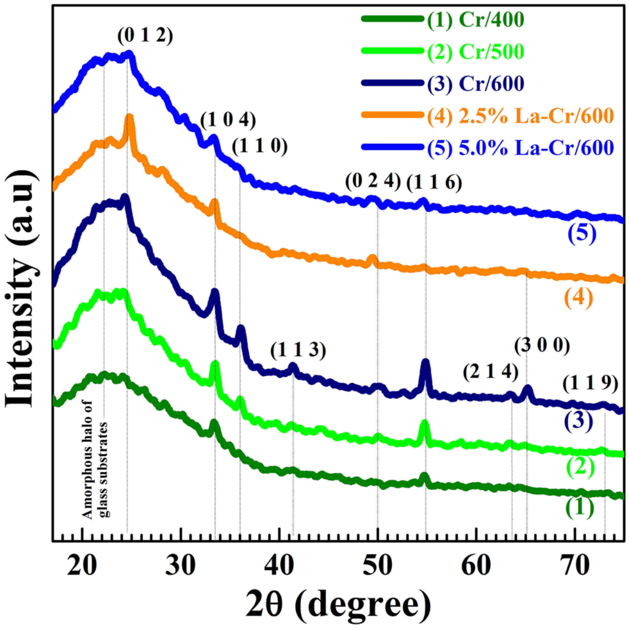

Figure 1: XRD patterns of chromia films annealed at 400, 500, and 600°C and doped with 2.5 and 5.0 at% La.

doped CuO [31] and Co_3O_4 [32]. La doping resulted in a peak shift that was observed for (0 1 2), (02 4), and (1 1 6) planes, indicating the successful replacement of Cr with La atoms. The smaller Cr atoms (r_{Cr} = 0.615 Å) [33,34]) in the host lattice were substituted by larger La atoms (r_{La} = 1.19 Å [34]), so that the host atoms suffered compression, and the lattice parameters contracted, resulting in a compressive strain [20].

The crystallite size C_s was determined using the well-known Scherrer equation: $C_s(\mathrm{nm}) = \frac{K \times 0.154}{\mathrm{FWHM}x\ \cos\theta}$, where Scherrer's constant K = 0.89 and 0.154 for the wavelength of the used Cuk_α. The obtained C_s values are listed in Table 1. HT from 400 to 600°C resulted in an increase in the C_s value from 24 to 38 nm, while La doping reduced it to 16 nm at a content of 5.0% La. Similarly, loading of 15 and 30% Ba reduced the C_s of sol–gel-derived chromia from 24 nm to 15.7 and 15.2 nm, respectively [22]. The C_s determined for the spin-coated $Cu_{0.94}Ni_{0.06}O$ and $Cu_{0.88}Ni_{0.06}La_{0.06}O$ films were 24.2 and 11.35 nm, respectively [31]. Additionally, the C_s of the sol–gel-prepared $(La_2O_3)_{99.5}{\cdot}(Cr_2O_3)_{0.5}$ composite increased from 10 to 30 nm with the increase of the HT temperature from 100 to 850°C [35]. In contrast to these results, the XRD patterns of the tapioca-assisted sol–gel-prepared chromia doped with Fe up to 18% showed no impurity peaks, and the C_s value increased from approximately 30 to 76 nm [33]. The C_s values of co-precipitated chromia decreased from 37.5 nm for the undoped sample to 28.1 nm at 2.0% Sr level but increased to 56.6 nm at 6.0% Sr content. Besides the Cr_2O_3 phase, the obtained chromia films were found to contain Cr_2O_5 and Cr_8O_{13} phases. This indicates that the sol–gel/spin coating methods can provide pure films. Moreover, the Y/Cr_2O_3 multilayered films prepared by ion-plating technology exhibited a (104) preferential growth. Some Cr and $Cr_2O_{2.4}$ peaks were observed due to O_2 deficiency during film deposition, and the element Y was also detected when its content reached 12.23% [5].

The assessment of chemical (reactive) groups in the prepared chromia and La-doped chromia films was done *via* recording FTIR spectra in the wavenumber range (400–4,000 cm^{-1}), as shown in Figure 2. The vibrations of metal–oxygen (Cr–O) bonds are prominent in the 400–1,000 wavenumber region because of the interatomic vibrations [3]. The inset of Figure 2 displays magnified vibration bands of chromia films annealed at 400°C (Cr/400) occurring at 500, 750, and 890 cm^{-1}. These peaks are assigned to stretching vibrations of Cr–O and Cr═O, as indicated in the figure. Besides, the less intense peak at 1,100 cm^{-1} can be assigned to Cr–O– Cr. The HT of the films at 500 and 600°C resulted in wider bands with higher intensity, with a significant shift of the 500 and 750 cm^{-1} bands to 486 and 765 cm^{-1}, respectively. However, the bands' intensity decreased upon La doping.

Investigating the exact position and intensity of Cr–O, Cr–O–Cr, and Cr═O vibrations is a controversial topic. In

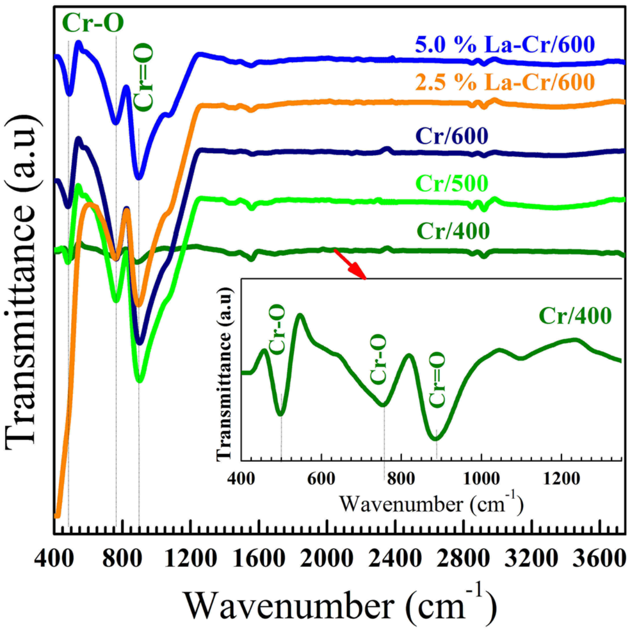

Figure 2: Transmittance (FTIR) spectra of chromia films heat-treated at 400–600°C and doped with 2.5 and 5.0 at% La.

Table 1: Crystallite size (C_s), transmittance (T%), optical band gap (E_g), $\frac{N}{m^*}$ ratio, and lattice dielectric parameter (ε_L) of chromia films heat-treated at 400–600°C and doped with 2.5 and 5.0 at% La

Film	C_s (nm)	T (%)		E_g (eV)	$\left(\frac{e^2}{\pi c^2}\right)\left(\frac{N}{m^*}\right)$	ε_L	R_{sheet} (kΩ)
		at λ = 380 nm	at λ = 500 nm				
Cr/400	24	46	68	2.70	1.052×10^{-6}	4.44	27.12
Cr/500	29	57	72	2.80	1.034×10^{-6}	3.87	31.64
Cr/600	38	64	78	2.90	0.313×10^{-6}	3.50	113
2.5% La-Cr/600	22	59	83	2.85	0.281×10^{-6}	3.20	90.4
5.0% La-Cr/600	16	50	80.5	2.75	0.391×10^{-6}	3.35	45.2

the Fe-doped Cr_2O_3 NPs prepared by the sol–gel route, Cr–O vibrational modes are located at 540 and 583 cm^{-1} [24]. Gyawali *et al.* [3] reported peaks for Cr–O bond stretching in the liquid-impregnated chromia NPs at 417 and 542 cm^{-1}. Alshammari and his group [22] noted peaks for Cr–O stretching in the sol–gel-prepared chromia NPs at 513 and 615 cm^{-1}. Also, they observed absorption peaks at 1,020 and 942 cm^{-1}, which arose from Cr–O–Cr and Cr–O vibrations, respectively. Ishtiaq *et al.* [20] claimed that peaks for Cr–O stretching vibrations in the spray-deposited chromia and Cu-doped chromia films were observed at 611 and 827 cm^{-1}, while those for Cr=O and Cr–O–Cr were observed at 892 and 1,040 cm^{-1}, respectively. However, they detected vibrations related to C=O and H_2O molecules. In addition, Ashika *et al.* [10] detected small bands in the range of 1,450–4,000 cm^{-1} attributed to the water and carbonate species that are adsorbed at the surfaces of chromia NPs. This again confirms that the sol–gel/spin coating methods yield chromia films with high purity. According to Khatamian *et al.* [26], the chromia NPs prepared by alkaline melting of the chromite ore exhibit two intense bands at 571 and 626 cm^{-1} and less intense ones at 443 cm^{-1}, originating from the Cr–O stretching vibration. The peaks for Cr−O and Cr=O vibrations in the bio-synthesized chromia NPs were found at 610 and 836–901 cm^{-1}, respectively. Increasing/decreasing the sharpness and height of the peaks after HT/La doping is due to the improvement/deterioration of the films' crystallinity [3]. The absence of La bands is due to the small concentration of La in the doped films. No new bands such as La–O or La–Cr were observed, which means that there is no chemical interaction between La and Cr_2O_3 films. These results align with the XRD findings and validate the ability to adjust the structure of chromia films through incorporation of HT and La.

The film surface morphology and the chemical (elemental) composition of the spin-coated chromia films on glass substrates annealed at 400°C (Cr/400) and 600°C (Cr/600) and 5.0% La-doped chromia (5.0 % La-Cr/600) were investigated by FE-SEM and the EDX, as illustrated in Figures 3(a)–(c) and 4(a)–(c), respectively. The Cr/400 film has grains of size in the range of 35–56 nm and a large number of small cracks.

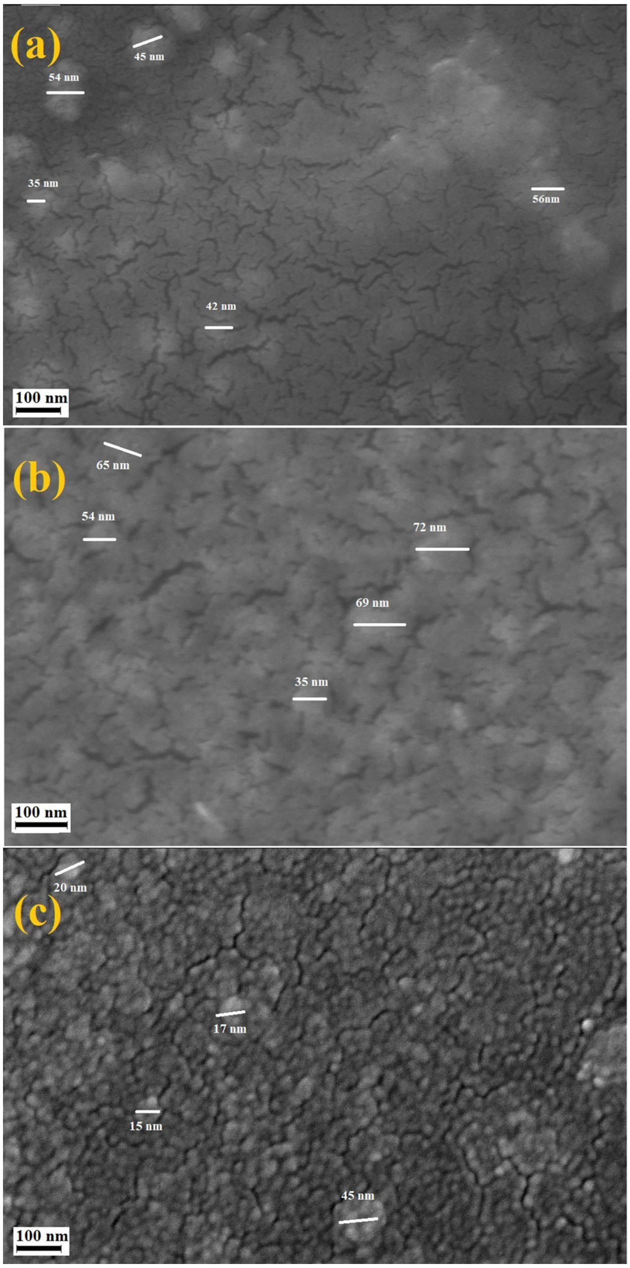

Figure 3: (a)–(c) FE-SEM surface images of Cr/400, Cr/600, and 5.0 %La-doped Cr/600 films.

These cracks may be formed during the pre-heating process due to solvent evaporation. Increasing the HT to 600°C resulted in grains with large sizes in the range of 45–72 nm and a reduced number of cracks. The 5.0% La doping had an impact on the film morphology, causing the grains to appear smaller and the zigzag (curved) cracks to have smaller widths. A similar morphology was observed for 2–10% La-doped TiO_2 [29]. This morphology increased the films' surface area for efficient performance in various applications such as gas sensing, photocatalysis, and water treatment. A similar finding was reported for DC-sputtered chromia films, whose nanoflake-like morphology changed into flat-surface morphology after Pd inclusion [18]. The grain size (and morphology) evaluated by high-resolution transmission electron microscopy (HR-TEM) for the sol–gel-prepared Fe-doped Cr_2O_3 NPs was found to decrease from 36.56 nm (ellipsoidal shapes) to about 22.84 nm (nanorod-like) at 10 at% Fe, which then grew to 66.5 nm (spherical shape) at 30 at% Fe [24]. Huiming *et al.*

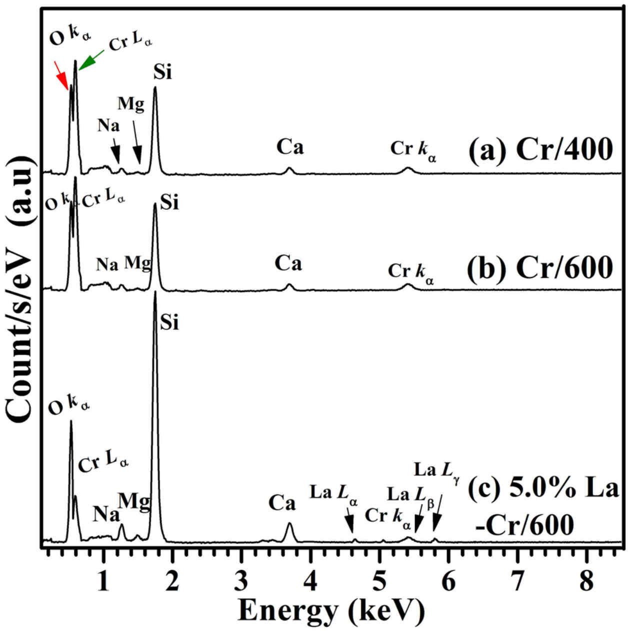

Figure 4: (a)–(c) Elemental analysis of Cr/400, Cr/600, and 5.0 %La-Cr/600 films.

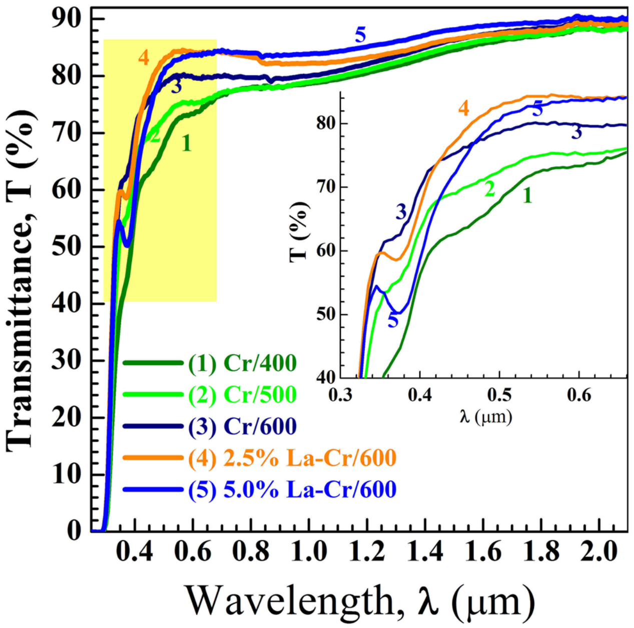

Figure 5: Optical T% for the spin-deposited chromia under HT and La doping.

[36] reported that La implantation at 3 × 10^{17} La ion/cm^2 on the Co–40Cr alloy at 10^3 promoted the formation of the Cr_2O_3 film with fine-grains.

Figure 4(a)–(c) shows EDX analyses of Cr/400, Cr/600, and 5.0% La-Cr/600, respectively. These EDX spectra indicate the existence of O and Cr peaks. Two peaks attributed to Cr are observed at around 0.58 keV (Cr L_α) and 5.4 keV (Cr K_α). The signal of O at 0.5 keV (O K_α) originates from the Cr_2O_3 films and also from the glass slides. Additionally, the Si (main component of glass), Na, Mg, and Ca signals are from the glass used as substrates. The EDX has a volume of interaction of about ≥ 1 µm (when the voltage of accelerating is ≥ 11 keV), which is larger than the film thickness [37]. The spectrum of 5.0% La-Cr/600 contains three (L_α, L_β, and L_γ) lines that confirms the presence of La at 4.6, 5.4, and 5.8 keV, respectively. The ratio [Cr]/[O] in Cr/400 and Cr/600 films appears to be the same. While the [Cr] is decreased relative to [O] upon doping with 5.0 at% La.

3.2 Film transmittance and band gaps

The UV–vis–NIR transmittance (T%) spectra are shown in Figure 5. T% increases sharply in the UV region, and at $\lambda \geq$ 400 nm all films exhibit 60–90% transmittance. The inset of this figure is a magnified view for T% values in the 320–660 nm wavelength range. The values at 380 and 500 nm for all films are displayed in Table 1. The T% values of the Cr/400 film at these two wavelengths are 46 and 68%, which increase to 64 and 78% with the increase of the AT to 600°C, and then became 50 and 80.5%, respectively, after doping the Cr/600 film with 5.0% La. This result illustrates that the T% of the chromia films is adjustable, where it increases with annealing, due to the improved films' crystallinity, and is lowered by La incorporation, where the defects induced by La absorb or scatter the incident photons. Optoelectronic and photovoltaic devices can harvest this high transmittance.

The films' absorption coefficient (α) can be derived from T% using the following equation: $\alpha = \frac{1}{d} \ln(1/T)$, where d is the film thickness. In addition, the value of α is dependent on the photon energy ($h\nu$) through Tauc's relationship: $(h\nu \times \alpha)^{\frac{1}{r}} = A(h\nu - E_g)$, where A is a constant and $r = \frac{1}{2}$ for the direct optical transition. Figure 6 shows the plots of $(\alpha h\nu)^2 vs h\nu$, where extending the linear parts of the obtained curves to $(\alpha h\nu)^2$ = zero (zero absorption) gives the values of E_g. The E_g of Cr/400 is found to be 2.7 eV, significantly increasing to 2.9 eV after annealing the films at 600°C. HT at high temperatures supply the atoms and molecules with the required thermal energy to occupy their normal (ideal) positions [38]. This increases the crystallinity and reduces the defects inside the material band gap. The E_g of the sputtered Cr_2O_3/CuO thin film at 100 W (200 W) increases from 2.33 (1.96) eV to 2.64 (2.47) eV under HT at increasing temperatures from 300 to 1,000°C. At 300 W, the E_g increases from 1.92 to 2.13 eV under HT at

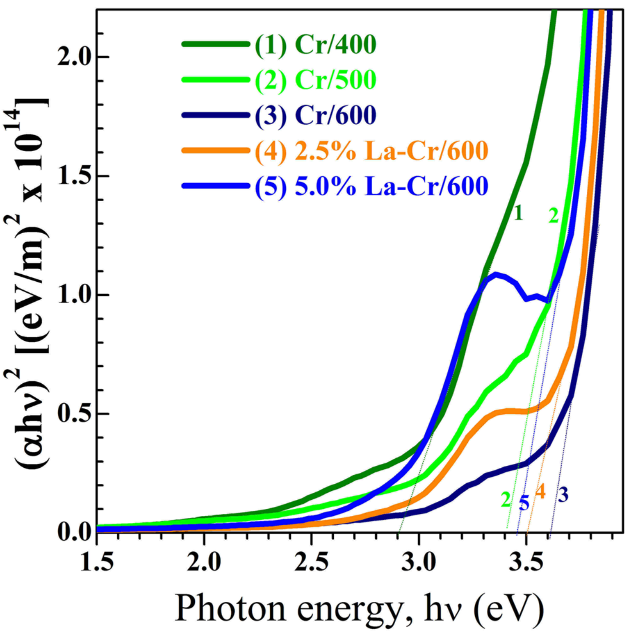

Figure 6: Tauc plot for E_g determination for the films under HT and La doping.

temperatures from 300 to 600°C and then decreases to 1.45 eV at 1,000°C [38]. At 300 W and 10,000°C, the high thermal energy may force the atoms to diffuse inside the substrate, which deteriorates the crystallinity.

La incorporation induces a reverse effect and narrows the E_g value from 2.9 to 2.75 eV. Doping with the La content produces defects or traps for the charge carriers and delays or inhibits their recombination, reducing the E_g value. Similarly, the E_g of ZnO decreases from 3.260 to 3.147 eV at 7.5 at% La content [25]. In addition, 0–12 at% Nb doping reduces the E_g of SnO_2 quantum dots from 4.76 to 2.18 eV [39]. In contrast, the E_g of the $Cu_{0.94}Ni_{0.06}O$ film increases from 1.5 to 2.3 eV when the film is codoped with 6.0 at% La ($Cu_{0.88}Ni_{0.06}La_{0.06}O$) [31]. The transparency and E_g of materials are affected by materials' structural geometry [16]. The decrease in T% with increasing La content from 2.5 to 5.0 at% could be due to the introduction of more La in the lattice sites into interstitial positions [40]. Increasing the La content results in more defects, disorders, and O vacancies that absorb a portion of the incident light and reduce the transmitted part. In addition, the difference in ionic radii between the host and dopant atoms increases the defect sites and generates charge carriers inside the band gap.

The literature reported similar findings, showing that doping with 3.0% Ag reduces the E_g value of ion-impregnated chromia NPs from 3.4 to 2.82 eV, resulting from the defect sites formed in the composite films [3]. Values of 1.82 ≤ E_g ≤ 2.3 eV were reported for chromia NPs prepared by hydrothermal, co-precipitation, thermal treatment, and ball milling under different synthetic conditions [10]. Fan *et al.* [12] reported that the PLD chromia thin films showed T% = 53–90% in the UV–vis spectra, and their E_g increased from 2.9 to 3.1 eV after doping with 5.0 at Ni. Bhardwaj *et al.* [16] reported a slight reduction in the E_g of chromia (from 3.61 to 3.56 eV) upon 5.0 at% doping with Ni, Mn, or Co, due to some structural distortions originating from the charge disproportion. Alshammari *et al.* [22] reported a band gap of 3.28 eV for the sol–gel chromia NPs, measuring 25 nm in size, which decreased to 2.8 and 1.5 eV upon loading 15 and 30% Ba. Chromia NPs prepared by the co-precipitation method showed a direct E_g of 3.3 eV, shifted toward 3.0 eV upon doping with 2, 4, and 6.0% Sr [23]. The band gaps of chromia and chromia/bentonite were found to be the same (3.09 and 3.08 eV) [26]. Addition of 45% Ti decreased the E_g of ALD chromia from 3.1 to 2.2 eV [27]. The direct (indirect) E_g of TiO_2 decreased from 3.38 (3.24) eV to 3.26 (2.53) eV at 4.0% La [29], then increased to 3.52 (3.02) eV at 10 % La. Tuning of this E_g broadened the films' utilization for photovoltaic and optoelectronic devices [31]. The spray-deposited chromia films demonstrated 65% transmittance, which improved to 94% by In doping at 4.0 at% content. The C_s and E_g values of 2.0% In content increased from 23 nm and 3.6 eV to 29 nm and 3.93 eV upon increasing [In] to 4.0% and then decreased to 3.46 eV at 8.0% In [40]. Moreover, the E_g value of the spray-pyrolyzed chromia decreased from 2.92 to 2.63 eV when doped with 4.0% Cu [41]. In contradiction to these results, Nikolaev *et al.* [4] reported an E_g of 3.06 eV for the undoped chromia layer grown by mist-CVD epitaxy, which then increased from 3.16 to 3.73 eV with increasing Ga content in the $(Cr_{1-x}Ga_x)_2O_3$ structure from $x = 0.03$ to 0.5. Loading 0–10 at% Cu through the microwave-assisted technique decreased C_s from 13.96 to 11.13 nm and increased the E_g of Cr_2O_3 NPs from 3.164 to 3.585 eV [42].

3.3 Chromia films' optical constants

Evaluating optical constants such as the absorption index (k, where $k = \frac{\lambda \times \alpha}{4\pi}$) and refractive index ($n$) are essential for optical communication and optoelectronic devices. Figure 7 shows the k distribution in the λ range of 280–1,750 nm. First, k values are high in both the UV and NIR regions, compared with those in the visible wavelengths. Second, Cr/400 exhibits two bands at 465 and 625 nm, which are related to the six-coordinated ${}^4A_{2g} \rightarrow {}^4T_{1g}$ and octahedral ${}^4A_{2g} \rightarrow {}^4T_{2g}$ of d^3 intrinsic electronic transitions for Cr^{3+} [43]. The d–d transitions from t_{2g} (triple

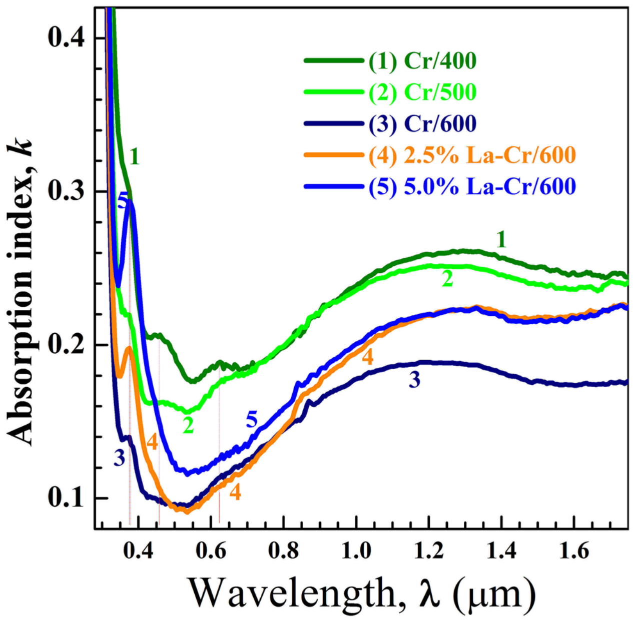

Figure 7: Absorption index dependence on the HT (400–600°C) and La content in chromia films.

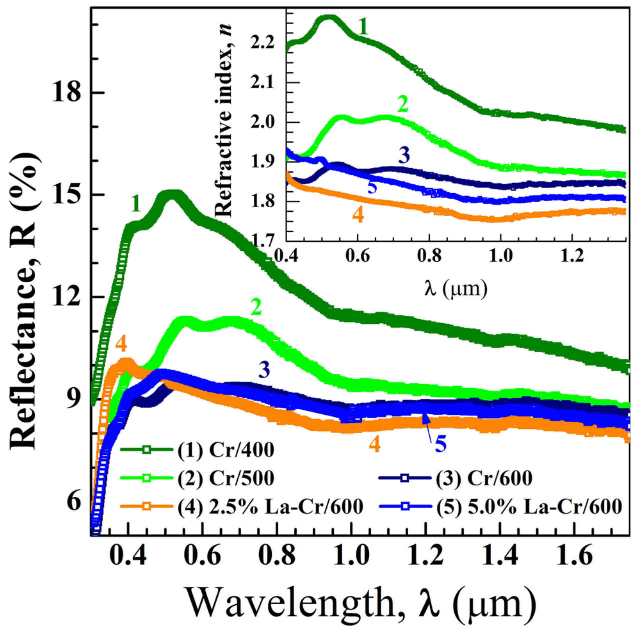

Figure 8: Dependence of reflectance *R* (%) and refractive index *n* (the inset) on HT and La content.

degenerate) to e_g (double degenerate) levels originate for these peaks and induce the green color of chromia [10]. Third, the absorption edge at 370 nm signifies the E_g of chromia [23]. This edge becomes clearer with the increase of the temperature from 400 to 600°C and becomes a band with enhanced intensity upon doping with La. In other words, the edge (band) at 370 nm grows in intensity at the expense of the other two bands at 465 and 625 nm. Fourth, the k values decrease with increasing AT and then increase with increasing La content from 0 to 5.0 at%. The behavior of k is related to the change in the film surface morphology, the increase/decrease in the crystallinity, and the available number of charges to absorb the incident light. This finding suggests that chromia-based IR sensors could be developed by controlling the AT and La content.

Figure 8 shows the dependence of the films' reflectance (R%) on the temperature and La doping. Materials with a larger number of particles exhibit higher reflectivity. Increasing the AT from 400 to 600°C results in increasing particle (grain) size, see Figure 3(a) and (b), where the particle tends to coalesce and thus reduces the number of particles. However, La doping leads to a reduction in the particle size, as revealed by XRD and SEM images. La-doped chromia appears with a large number of particles, each particle acting as a scattering or reflecting center. The n values are derived from R and k using the relation: $n = \frac{\sqrt{4R-(1-R)^2k^2}+R+1}{(1-R)}$ [44]. The inset of Figure 8 shows the n *vs* λ plot in the visible and NIR (400–1,350 nm) spectral regions. The n values of Cr/400 of 1.97–2.27 decrease to 1.85–1.9 with increasing AT to 600°C. The n values of the 2.5% La-Cr/600 film improve from 1.77–1.85 to 1.80–1.925 as the La content is increased. For all films, the highest n values correspond to λ equal to 525 and 670 nm. This behavior may be due to the fact that the incident photon frequency is equal to the plasma frequency [18]. The higher values of n for Cr/400 are due to the limited crystallinity and existing traps and disorders, which cause a higher level of photon scattering and reduced T%. These results are consistent with XRD and FE-SEM analyses.

Another two optical constants, the lattice dielectric constant (ε_L) and ($\frac{\text{carrier concentration}N}{\text{electron effective mass}m^*}$), can be determined from the dispersion relation: $n^2 = \varepsilon_L - \left(\frac{e^2}{\pi c^2}\right)\left(\frac{N}{m^*}\right)\lambda^2$ [42], where e and c are the electron charge and light speed, respectively. Figure 9 shows the n^2 *vs* λ^2 plots for all films. Extending the curves to meet the y-axis gives ε_L values, and the slope represents $\frac{N}{m^*}$ in terms of $\frac{e^2}{\pi c^2}$. The deduced values of $\frac{N}{m^*}\left(\frac{e^2}{\pi c^2}\right)$ and ε_L are given in Table 1. With the increase of the AT, both ε_L and $\frac{N}{m^*}$ decrease from 4.44 and 1.052×10^{-6} to 3.5 and 0.313×10^{-6}, respectively. When the Cr/600 film is doped with 5.0% La, the $\frac{N}{m^*}$ value increases to 0.391×10^{-6}. The decrease/increase of $\frac{N}{m^*}$ with AT/La doping is consistent

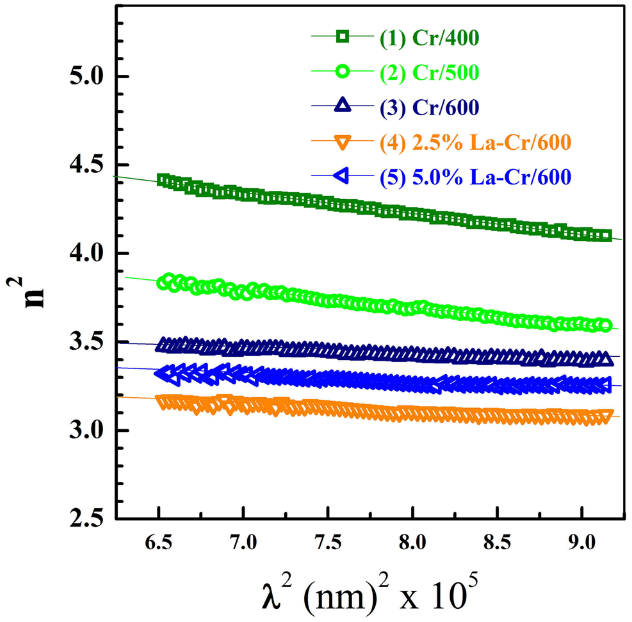

Figure 9: n^2 *vs* λ^2 plot for determining the $\frac{N}{m^*}$ and ε_L optical parameters.

with the increase/decrease of the E_g of the films. The obtained results confirm that the optoelectronic properties of the chromia films can be controlled by changing the experimental conditions (HT) and doping approach. The chromia films are therefore the best candidates for designing optical filters with a reasonable E_g.

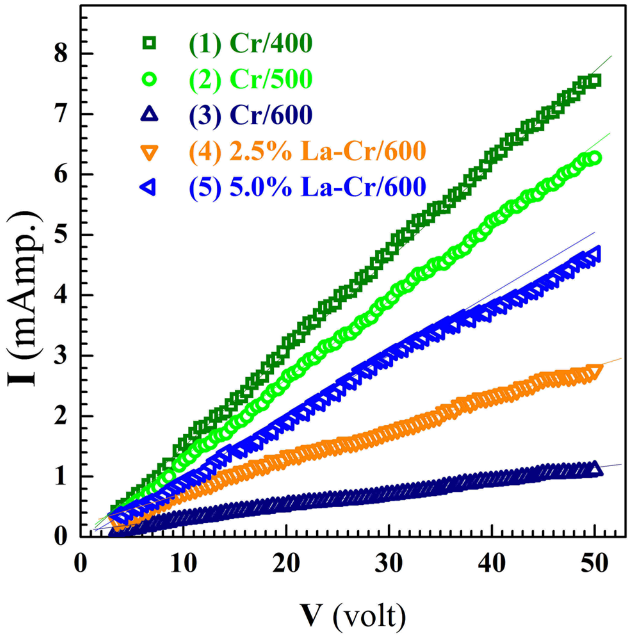

Figure 10: I–V characteristic curves of chromia films annealed at different temperatures and doped with La.

3.4 I–V characteristic curves

Figure 10 shows the I–V plots of the spin-deposited chromia films on the glass substrate. The linear I–V curves indicate good Ohmic resistance. Bhardwaj *et al.* [16] also found a linear I–V relationship for chromia doped with Ni, Co, and Mn that was deposited on Al_2O_3 substrates. The films' sheet resistance (R_{sheet}) was calculated from the slope ($\frac{\Delta I}{\Delta V}$) of the equation: $R_{\text{sh}} = \frac{\pi}{\ln 2}\frac{1}{\text{slope}} = \frac{4.532}{\text{slope}}$ [41], where 4.532 is the correction factor. The R_{sheet} values, Table 1, are high (27.12–113 kΩ). These values are higher than those reported for the spray pyrolyzed films [40]. The smallest R_{sheet} value was exhibited by the film that was annealed at 400°C. The R_{sheet} value increased with increasing AT, which then decreased upon La loading. During annealing, the atoms and molecules get sufficient thermal energy for more arrangement and occupying the ideal positions. However, La introduces more disordering and defect states in the material's band gap. Therefore, this change in R_{sheet} is consistent with the variation in films' E_g values. The resistivities of the spray-deposited chromia and 4.0% Cu-doped chromia films were found to be 960 and 33.06 Ω cm, respectively [41]. This variation in R_{sheet} values is related to the change in films' crystallinity, morphology, and chemical composition.

4 Conclusions

The influence of HT at temperatures in the range of 400–600°C and La incorporation on the physical properties of chromia thin films spin-deposited on glass substrates was investigated. XRD showed that hexagonal chromia was formed after annealing at 400°C. Raising the temperature to 600°C enhanced the films' crystallinity and increased the C_s value from 24 to 38 nm, which then dropped to 16 nm upon doping with 5.0% La. The Cr–O and Cr═O stretching vibrations of chromia were detected at 500, 750, and 890 cm^{-1}. Increasing the AT (increasing the La content) resulted in a small shift of these bands, and their intensity increased (decreased) based on the changes in the films' crystallinity. FE-SEM revealed that the films are formed from grains separated by a large number of small cracks. EDS spectra confirmed the existence of La in the film composition. UV–vis–NIR spectra revealed that HT in the range of 400–600°C improved T% from 46 to 64%, which then decreased to 50% due to La doping. The E_g increased from 2.7 to 2.9 eV and then reduced to 2.75 at 5.0% La. The films showed high absorption indices in the

UV and NIR regions. The R% and n oscillated between 6 and 15% and 1.77 and 1.97, respectively. In addition, the ε_L of the films was in the range of 3.2–4.44, and $\frac{N}{m^*}(\frac{e^2}{\pi c^2})$ was found to decrease from 1.052×10^{-6} to 0.313×10^{-6} after HT and increase to 0.391×10^{-6} upon addition of 5.0 at% La. The films displayed linear I–V curves (good Ohmic resistance) and R_{sheet} in the range of 27.12–113 kΩ. In summary, it is possible to engineer the films' crystallinity, morphology, band gap, optical constant, and resistance of the chromia films by HT and La content. Tuning the structure and optical and electrical properties of the chromia films widen their utilization in the practical and technological applications in the fields of optoelectronics, photonic devices, and chromia-based IR sensors. However, more studies are required on chromia films on Si or sapphire substrates for HT at higher temperatures than 600°C and the possible device fabrication and characterization.

Acknowledgments: The authors extend their appreciation to the Deanship of Scientific Research at Northern Border University, Arar, KSA, for funding this research work through the project number NBU-FFR-2025-310-05.

Funding information: This work was funded by the Deanship of Scientific Research at Northern Border University, Arar, KSA, through the project number NBU-FFR-2025-310-05.

Author contributions: Adel M. El Sayed: conceptualization, methodology, data curation, writing of the original draft, and editing of the manuscript. Faisal Katib Alanazi: methodology, data curation and investigation, and reviewing and editing of the revised manuscript. All authors have accepted responsibility for the entire content of this manuscript and approved its submission.

Conflict of interest: The authors state no conflict of interest.

Data availability statement: All data generated or analyzed during this study are included in this published article.

References

[1] Mbam SO, Nwonu SE, Orelaja OA, Nwigwe US, Gou X-F. Thin-film coating; historical evolution, conventional deposition technologies, stress-state micro/nano-level measurement/models and prospects projection: A critical review. Mater Res Express. 2019;6:122001. doi: 10.1088/2053-1591/ab52cd.

[2] Devan RS, Patil RA, Lin J-H, Ma Y-R. One-dimensional metal-oxide nanostructures: Recent developments in synthesis, characterization, and applications. Adv Funct Mater. 2012;22:3326–70. doi: 10.1002/adfm.201201008.

[3] Gyawali N, Kandel R, Lee I, Shrestha S, Pandey A, Akter J, et al. Silver decoration of Cr_2O_3 nanoparticles: Facile preparation of Cr_2O_3 nanoparticles and Ag–Cr_2O_3 nanocomposites and characterization of their antibacterial activity and ability to photocatalytically degrade organic wastes under visible light. J Photochem Photobiol A: Chem. 2024;447:115251. doi: 10.1016/j.jphotochem.2023.115251.

[4] Nikolaev VI, Shapenkov SV, Timashov RB, Stepanov AI, Scheglov MP, Chikiryaka AV, et al. High-quality Cr_2O_3 - Ga_2O_3 solid solutions films grown by mist-CVD epitaxy. J Alloy Compd. 2024;994:174687. doi: 10.1016/j.jallcom.2024.174687.

[5] Jia B, Xu W, Li J, Liu X, Ji L, Sun C, et al. Enhancement of thermal stability and high-temperature oxidation resistance of chromium oxide-based films by addition of rare earth element Y. J Mater Sci Technol. 2024;188:105–15. doi: 10.1016/j.jmst.2023.11.034.

[6] Tian T, Zheng L, Bernik S, Man Z, Shi X, Ruan X, et al. Influence of Cr_2O_3 doping on the electrical characteristics of novel ZnO-Cr2O3-based varistor ceramics. Mater Res Bull. 2023;159:112111. doi: 10.1016/j.materresbull.2022.112111.

[7] Li L, Cheng J, Zhao Q, Zhang J, Yang H, Zhang Y, et al. Chromium oxide film for Q-switched and mode-locked pulse generation. Opt Express. 2023;31(10):16872–81. doi: 10.1364/OE.491792.

[8] Alotabi AS, Small TD, Yin Y, Osborn DJ, Ozaki S, Kataoka Y, et al. Reduction and diffusion of Cr-oxide layers into P25, $BaLa_4Ti_4O_{15}$, and Al:$SrTiO_3$ particles upon high-temperature annealing. ACS Appl Mater Interfaces. 2023;15(11):14990–15003. doi: 10.1021/acsami.3c00250.

[9] Hossain MI, Mansour S. A critical overview of thin films coating technologies for energy applications. Cogent Eng. 2023;10:2179467. doi: 10.1080/23311916.2023.2179467.

[10] Ashika SA, Balamurugan S, Sana Fathima TK, Palanisami N, Viswanathan T. Detailed studies on the synthesis methods and characterizations of nanocrystalline Cr_2O_3 phase materials for NIR pigmentation applications. ECS J Solid State Sci Technol. 2023;12:053004. doi: 10.1149/2162-8777/acd210.

[11] Tsegay MG, Gebretinsae HG, G.Welegergs G, Maaza M, Nuru ZY. Novel green synthesized Cr_2O_3 for selective solar absorber: Investigation of structural, morphological, chemical, and optical properties. Sol Energy. 2022;236:308–19. doi: 10.1016/j.solener.2022.03.011.

[12] Fan Z, Zhu M, Pan S, Ge J, Hu L. Giant photoresponse enhancement in Cr2O3 films by Ni doping-induced insulator-to-semiconductor transition. Ceram Int. 2021;47:13655–59. doi: 10.1016/j.ceramint.2021.01.226.

[13] Erickson A, Shah SQA, Mahmood A, Buragohain P, Fescenko I, Gruverman A, et al. Imaging local effects of voltage and boron doping on spin reversal in antiferromagnetic magnetoelectric Cr_2O_3 thin films and devices. Adv Funct Mater. 2024;34:2408542. doi: 10.1002/adfm.202408542.

[14] Goel S, Kumar A, Quamara JK, Kumar J. Structural, optical and magnetic properties of Fe doped Cr_2O_3 nanoparticles. Adv Sci Lett. 2014;20:1562–6. doi: 10.1166/asl.2014.5576.

[15] Bhardwaj P, Kumar R, Singh J, Verma V, Kumar R. A comparative study on the structural, optical, and magnetic behavior of

transition metal (Co and Mn) ions substituted Cr_2O_3 nanoparticles. J Magn Magn Mater. 2023;565:170247. doi: 10.1016/j.jmmm.2022.170247.

[16] Bhardwaj P, Singh J, Singh AP, Choudhary RJ, Verma V, Kumar R. Observation of room temperature ferromagnetism in transition metal ions substituted p-type transparent conducting oxide Cr_2O_3 thin films. Mater Sci Eng: B. 2024;299:116990. doi: 10.1016/j.mseb.2023.116990.

[17] Yıldırım GB. Investigation of electrochemical performance of Ni/Cr_2O_3 and Co/Cr_2O_3 composite nanoparticles prepared by microwave-assisted solvothermal method. J Alloy Compd. 2023;960:170627. doi: 10.1016/j.jallcom.2023.170627.

[18] Rani R, Sharma M, Sharma S, Chandra R, Malik VK. Palladium enhanced electrochemical supercapacitive performance of chromium oxide thin films synthesized by sputtering process. Thin Solid Films. 2024;799:140379. doi: 10.1016/j.tsf.2024.140379.

[19] Zekaik A, Benhebal H, Benrabah B. Synthesis and characterization of Cu doped chromium oxide (Cr_2O_3) thin films. Temp Mater Process. 2019;38:806–12. doi: 10.1515/htmp-2019-0037.

[20] Ishtiaq M, Ali D, Ahmad R, Muneer I, Bashir F, Hanif M, et al. A comparison of antibacterial activity in dark-UV light in perspective of surface and structural properties of spray pyrolysis grown Cu doped Cr_2O_3 thin films. Surf Interfaces. 2023;37:102741. doi: 10.1016/j.surfin.2023.102741.

[21] Yasmeen G, Hussain S, Tajammal A, Mustafa Z, Sagir M, Shahid M, et al. Green synthesis of Cr_2O_3 nanoparticles by Cassia fistula, their electrochemical and antibacterial potential. Arab J Chem. 2023;16:104912. doi: 10.1016/j.arabjc.2023.104912.

[22] Alshammari K, Alotibi S, Alhassan S, Alshammari M, Alshammari AH, Alotaibi T, et al. Preparation of chromium barium oxide catalysts for hydrogen evolution from sodium borohydride methanolysis. J Ind Eng Chem. 2024;136:229–36. doi: 10.1016/j.jiec.2024.02.010.

[23] Ikram M, Shahzadi A, Bilal M, Haider A, Ul-Hamid A, Nabgan W, et al. Strontium-doped chromium oxide for RhB reduction and antibacterial activity with evidence of molecular docking analysis. Front Chem. 2023;11:1167701. doi: 10.3389/fchem.2023.1167701.

[24] Attah-Baah JM, Santos C, Silva RS, Jr., Oliveira JL, Jucá RF, Costa BFO, et al. Unveiling the impact of Fe-doping concentration on the local structure and morphological evolution of Cr_2O_3 nanoparticles. Ceram Int. 2024;50:35714–24. doi: 10.1016/j.ceramint.2024.06.389.

[25] Shaban M, El Sayed AM. Effects of lanthanum and sodium on the structural, optical and hydrophilic properties of sol–gel derived ZnO films: A comparative study. Mater Sci Semiconductor Process. 2016;41:323–34. doi: 10.1016/j.mssp.2015.09.002.

[26] Khatamian M, Dastar E, Fazli-Shokouhi S, Hosseini Nami S. Synthesis of pure nano Cr_2O_3 from chromite ore by a novel method and investigation of its composites with bentonite for their photocatalytic properties. J Iran Chem Soc. 2023;20:2805–19. doi: 10.1007/s13738-023-02877-9.

[27] Salari Mehr M, Aarik L, Jõgiaas T, Kasikov A, Damerchi E, Mändar H. Mechanical and optical properties of Cr_2O_3 thin films grown by atomic layer deposition method using $Cr(thd)_3$ and Ozone. Nanomaterials (Basel, Switz). 2023;13:2702. doi: 10.3390/nano13192702.

[28] Salari Mehr M, Aarik L, Jõgiaas T, Tarre A, Kasikov A, Roosalu K, et al. Ti doped Cr_2O_3 thin films: Atomic layer deposition, mechanical and optical properties. J Alloy Compd. 2023;968:172041. doi: 10.1016/j.jallcom.2023.172041.

[29] Joshi P, Tiwari S, Kumar S. A comprehensive study on the impact of La doping on the microstructural, optical, luminescence and magnetic characteristics of greenly synthesized LaxTi1-xO2 QDs. Appl Phys A. 2025;131:88. doi: 10.1007/s00339-024-08207-x.

[30] Shi M, Zhang L, Cheng Z, Wang Z, He Q, Qin J, et al. Effect of La_2O_3 doping on microstructure and electrical properties of flash-sintered ZnO-Bi_2O_3 varistor. J Mater Sci: Mater Electron. 2022;33:23437–46. doi: 10.1007/s10854-022-09105-9.

[31] Khmissi H, El Sayed AM, Shaban M. Structural, morphological, optical properties and wettability of spin-coated copper oxide; influences of film thickness, Ni, and (La, Ni) co-doping. J Mater Sci. 2016;51:5924–38. doi: 10.1007/s10853-016-9894-7.

[32] Shaban M, El Sayed AM. Influence of the spin deposition parameters and La/Sn double doping on the structural, optical, and photoelectrocatalytic properties of $CoCo_2O_4$ photoelectrodes. Sol Energy Mater Sol Cell. 2020;217:110705. doi: 10.1016/j.solmat.2020.110705.

[33] Santos C, Attah-Baah JM, Junior RSS, Mâcedo MA, Rezende MVS, Matos RS, et al. Insights into the Fe^{3+} Doping Effects on the Structure and Electron Distribution of Cr_2O_3 Nanoparticles. Nanomaterials (Basel, Switz). 2023;13:980. doi: 10.3390/nano13060980.

[34] El Sayed AM, Shaban M. Morphological, surface and optical properties of spin-coated IrOx films; influence of spin speed, annealing and (Cr, La) codoping. Ceram Int. 2019;45:8460–70. doi: 10.1016/j.ceramint.2019.01.156.

[35] Simon S, Simon V. Heat treatment effect on nanostructured sol-gel derived lanthania doped with chromium. J Non-Crystalline Solids. 2021;555:120624. doi: 10.1016/j.jnoncrysol.2020.120624.

[36] Huiming J, Xiaowei Z, Linnan Z. Effects of lanthanum ion-implantation on microstructure of oxide film formed on Co-Cr alloy. J Rare Earths. 2008;26(3):406–9. doi: 10.1016/S1002-0721(08)60106-4.

[37] Shaban M, El Sayed AM. Influences of lead and magnesium co-doping on the nanostructural, optical properties and wettability of spin coated zinc oxide films. Mater Sci Semiconductor Process. 2015;39:136–47. doi: 10.1016/j.mssp.2015.04.008.

[38] Ponmudi S, Sivakumar R, Sanjeeviraja C. Tuning the phase structure and surface morphology of Cr2O3:CuO thin film by annealing for enhanced ammonia sensing performance at room temperature. Inorg Chem Commun. 2023;158:111512. doi: 10.1016/j.inoche.2023.111512.

[39] Liu J, Zhao D, Wu X, Wu D, Su N, Wang Y, et al. Synergistic dual-defect band engineering for highly efficient photocatalytic degradation of microplastics *via* Nb-induced oxygen vacancies in SnO_2 quantum dots. J Mater Chem A. 2025;13:4429–43. doi: 10.1039/d4ta07579j.

[40] Saadi B, Rahmane S, Temam EG. Structural, optical and electrical properties of spray deposited indium-doped Cr_2O_3 thin films. J Opt. 2024;53(1):582–9. doi: 10.1007/s12596-023-01252-4.

[41] Ishtiaq M, Ali D, Ahmad R, Muneer I, Khan TM. Tuning optical and electrical characteristics through Cu doping in spray pyrolysis fabricated Cr2O3 thin films. Opt Mater. 2024;148:114930. doi: 10.1016/j.optmat.2024.114930.

[42] Mohanapandian K, Kamala SSP, Periasamy P, Priya NS, Selvakumar B, Senthilkannan K. Cu^{2+} substituted Cr_2O_3

nanostructures prepared by microwave-assisted method: An investigation of its structural, morphological, optical, and dielectric properties. J Sol-Gel Sci Technol. 2021;99:546–56. doi: 10.1007/s10971-021-05596-w.

[43] Arca E, Fleischer K, Krasnikov SA, Shvets I. Effect of chemical precursors on the optical and electrical properties of p-type transparent conducting Cr_2O_3:(Mg,N). J Phys Chem C. 2013;117(42):21901–07. doi: 10.1021/jp404230k.

[44] El-Sayed S, Sayed AME. Preparation and characterization of CuO/Co_3O_4/poly(methyl methacrylate) nanocomposites for optical and dielectric applications. J Mater Sci: Mater Electron. 2021;32:13719–37. doi: 10.1007/s10854-021-05949-9.